

# Learning a Gauge Symmetry with Neural-Networks

A. Decelle,<sup>1</sup> V. Martin-Mayor,<sup>2,3</sup> and B. Seoane<sup>4,5</sup>

<sup>1</sup>Laboratoire de Recherche en Informatique, TAU - INRIA, CNRS,  
Université Paris-Sud et Université Paris-Saclay, Bât. 660, 91190 Gif-sur-Yvette, France

<sup>2</sup>Departamento de Física Teórica, Universidad Complutense, 28040 Madrid, Spain

<sup>3</sup>Instituto de Biocomputación y Física de Sistemas Complejos (BIFI), 50018 Zaragoza, Spain

<sup>4</sup>Sorbonne Université, CNRS, IBPS, UMR 7238,

Laboratoire de Biologie Computationnelle et Quantitative (LCQB), 75005 Paris, France

<sup>5</sup>Sorbonne Université, Institut des Sciences, du Calcul et des Données (ISCD), 75005 Paris, France

(Dated: April 17, 2019)

We explore the capacity of neural networks to detect a symmetry with complex local and non-local patterns : the gauge symmetry  $Z_2$ . This symmetry is present in physical problems from topological transitions to QCD, and controls the computational hardness of instances of spin-glasses. Here, we show how to design a neural network, and a dataset, able to learn this symmetry and to find compressed latent representations of the gauge orbits. Our method pays special attention to system-wrapping loops, the so-called Polyakov loops, known to be particularly relevant for computational complexity.

The physics community is now greatly excited by the possibilities offered by machine learning tools, which have reached *superhuman* performance in tasks of significant complexity (think, for instance, of Go playing [1]). Indeed, deep (convolutional) neural networks (DNN or DCNN) [2, 3], initially developed for classification and pattern recognition tasks, have been applied to the identification of phases of matter [4–10], including structural glasses [11–13] and topological states [14], or even to seemingly for-humans-only tasks, such as finding real-space renormalisation group transformations [15] (this is just a somewhat arbitrary selection of, literally, hundreds of applications to physics).

In this context, gauge symmetries pose a major challenge due to the absence of any local order parameter [16], which explains why only preliminary studies have been conducted [5, 6] (this paper adds to this list). It is natural to study gauge symmetries using DCNN because thanks to the convolutional layer, the translational symmetry has been successfully exploited in image recognition: if a previously learned imaged is moved, less advanced algorithms fail to recognize it. Now DNN encodes the translational symmetry at a local level using a specific architecture (the convolutional layers), and therefore the obvious next step for Physicists is to consider more general symmetries for practical purpose.

The specific question we had in mind was whether or not DNN could be used to predict the *computational complexity* of a particular instance of an optimization problem. Spin glasses represent the perfect playground to test this idea, because finding the ground state of a simple Hamiltonian such as:

$$\mathcal{H} = - \sum_{\langle \mathbf{x}, \mathbf{y} \rangle} J_{\mathbf{x}\mathbf{y}} \sigma_{\mathbf{x}} \sigma_{\mathbf{y}}, \quad (\sigma_{\mathbf{x}} = \pm 1 \text{ for all sites } \mathbf{x}), \quad (1)$$

is an NP-complete problem as soon as the underlying interaction-graph is non-planar [17, 18] (we shall con-

sider statistically independent couplings  $J_{\mathbf{x}\mathbf{y}} = \pm 1$  with 50% probability). The classification problem is motivated because the computational difficulty of solving different problem instances of Eq. (1) spreads over several orders of magnitude [19–24], even for such a modest number of spins as  $N \sim 500$  [25]. It is still unknown which features of the coupling matrix  $J_{\mathbf{x}\mathbf{y}}$  cause this tremendous disparity of computational cost, in spite the obvious practical relevance of the question (see [21] for some attempts to answer it). DNNs would be an obvious choice to address the computational-cost classification problem, were it not for the gauge symmetry of Hamiltonian (1) (the  $\epsilon_{\mathbf{x}} = \pm 1$  are arbitrary) [26]

$$\tilde{J}_{\mathbf{x}\mathbf{y}} = J_{\mathbf{x}\mathbf{y}} \epsilon_{\mathbf{x}} \epsilon_{\mathbf{y}}, \text{ and } \tilde{\sigma}_{\mathbf{x}} = \epsilon_{\mathbf{x}} \sigma_{\mathbf{x}}. \quad (2)$$

All problem instances related by this transformation belong to the same *gauge orbit*. Now, the difficulty for solving problems from the same gauge orbit is *identical*. Hence, our dreamed DNN should first be able of telling us with certainty whether or not two problem instances belong to the same gauge orbit. Yet, we have checked that DNN, specifically ResNet [27], completely fails at this task, no matter the size of the training set.

Here we solve by means of a machine-learning algorithm the problem of gauge-orbit identification as formulated for spin glasses on the square lattice. The same algorithm works in the cubic lattice as well, although we are limited to systems of smaller linear size due to the memory and computational costs. Let us stress that a careless posing of the problem could make it (wrongly) seem trivial. The problem is naturally addressed in terms of Wilson loops, in our case, the product of the couplings along a closed loop in the lattice, which is gauge invariant, see e.g. Ref. [28]. Attention immediately falls on the shortest Wilson loop, named the *plaquette* (see e.g. [5] or Fig. 1–left). However, in Ref. [23] it is shown that two problem instances sharing the value of *every* plaque-

tte, but differing on the so-called Polyakov loops (Wilson loops wrapping the system thanks to the periodic boundary conditions), may have vastly different computational complexity. Of course, there are more complex loops than Polyakov’s, but we shall limit ourselves here to the simplest example. In fact, we have improved over Ref. [5] by teaching our machine to consider both local and non-local Wilson loops when studying a  $Z_2$  gauge symmetry.

Let us highlight two other aspects of this problem that machine-learning practitioners may find attractive: (i) training set of (essentially) arbitrary size can be easily generated and (ii) an algorithm of polynomial complexity provides an exact answer to the question of whether two problem instances belong to the same gauge orbit.

In the rest of the paper, we will present two different approaches to solve this classification problem using DNN. In the first part of the paper, we will show how to build a machine able to tell us if two samples are in the same gauge orbit. And in the second part, we will show how one can build an autoencoder, a DNN capable of finding a latent representation of a gauge orbit, and to fix approximately the gauge. The latent representation of the autoencoder can be used for classifying samples as in the first case, but it is much stronger, it actually allows us to cluster the samples by orbits. All the simulations were possible thanks to the Keras-tensorflow and scikit-learn libraries [29, 30]. Before going to the two methods, we explain how the data are prepared for the training procedure.

The fact of working with square lattices allows us to treat the coupling matrices as images and apply directly all the machinery developed for them. The construction of the images is done as follows: (i) we map our set of couplings to a new 2D euclidean lattice. This can be done in different ways, our choice was to double the initial size of the lattice, so that spins (not used for our images) would be located at once every two lattice spaces, so that the couplings  $J_{\mathbf{x}\mathbf{y}} = \pm 1$  (black/white in Fig. 1–left) in between them can be represented in the intermediate lattice sites. The rest of the sites not occupied by couplings are fixed to zero (grey in the Figure). This transformation will be named hereafter “chess transformation”. One could have avoided the introduction of all the useless grey pixels by just combining two square lattices of linear size  $L$ , but while we did not observe a particular advantage in the learning process when using this mapping, this choice complicated the interpretation of the results and the optimization of the machine, so we decided to keep the chess transformation. The periodic boundary conditions will be introduced in the final images given to the DNN, just by adding an extra row and column at the boundaries of the images with the information of its neighbors. For the sake of clarity, we do not include these extensions in the Figures shown.

We can now use this chess representation to illustrate

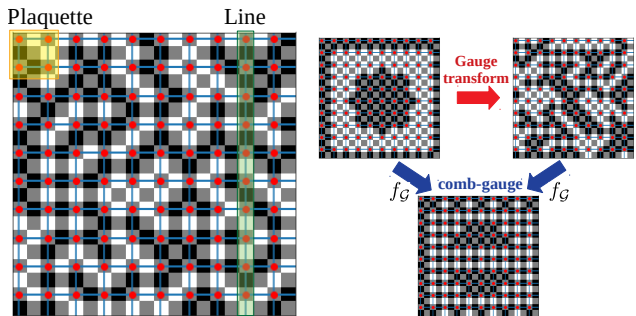


FIG. 1. (Left) Example of the chess transformation. The red dots indicate the spins location and the blue edges the links between them. The 2D grid fed to the neural network contains zero on all gray cells (spin nodes of empty nodes), and  $\pm 1$  values for the  $J_{\mathbf{x}\mathbf{y}}$ . (Right) Example of a possible sample and one of its gauge transforms. Both samples lead to the same comb gauge after gauge fixing.

the effect of a gauge transform, see Fig. 1–right. It is almost impossible to distinguish the second sample (which is a gauge transform of the first ordered sample) from a purely random sample by human eye. As mentioned above, the correct way to do it is to fix the gauge [31], that is, to use a map  $f_G : \mathcal{J}^{\mathcal{O}_k} \rightarrow \hat{\mathcal{J}}^{\mathcal{O}_k}$  from any sample  $\mathcal{J}$  of the gauge orbit  $\mathcal{O}_k$  to a single representation of it,  $\hat{\mathcal{J}}$ . Thus, two samples will be in the same orbit, if and only if  $f_G(\mathcal{J}^{\mathcal{O}_k}) - f_G(\mathcal{J}^{\mathcal{O}_l}) = 0$ . In practice, we construct this mapping by selecting the  $\epsilon \equiv \{\epsilon_{\mathbf{x}}\}$  values in Eq. (2) in a way that one can transform all the couplings along all the lines on the horizontal direction and on the first vertical line to 1 (black in the Figure). We call this particular gauge the *comb-gauge*. One can see that one has the freedom to do so along all these lines but for the last coupling at the end of each line due to the periodic boundary conditions. We include the code of this transformation in the Supplemental Material (SM).

**Construction of the data set**– A naive approach to detect the gauge symmetry (that was used in Ref. [5]) would consist in first constructing a (balanced) dataset of pairs of systems: a group which correspond to gauge symmetrical systems and a group with two random  $\mathcal{J}$ s. However one can already anticipate the problem that will arise from such a choice. The large majority of the times, and this is what the DNN will learn, the two samples will be so different that one could easily classify correctly these pairs just by checking the value of a very reduced number of plaquettes of the system. But this is not restrictive enough to check the gauge symmetry, it would completely miss situations in which just some few couplings have been changed, e.g.  $R_{q=0.05}(\mathcal{J})$  in Fig. 2, or more drastically, it would be blind to extensive transformation that leaves all the plaquettes unaltered, like the  $L(\mathcal{J})$  in Fig. 2. This example shows us that we need to be very careful when constructing the dataset if we want

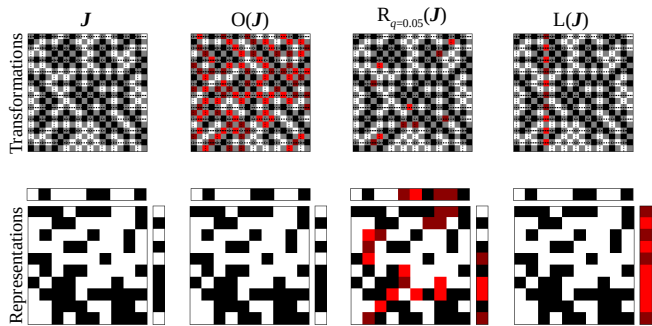


FIG. 2. The first row represents a sample  $\mathbf{J}$  and the possible transformations used to build our dataset. The second row corresponds to the sign of all the plaquettes in the system (i.e. product of the  $J_{ij}$  along the plaquette) and the sign of all the Polyakov loops (i.e. product of the  $J_{ij}$  along the horizontal and vertical lines). We highlight the pixels that change in red. For a given system  $\mathbf{J}$ , a random gauge transform changes most of the couplings but no plaquette or line, while changing some few links of a sample (see  $R_{q=0.05}$  where 5% of the couplings were flipped), has strong effects both in the plaquettes and the lines. The last column shows that, flipping a full vertical line of couplings does not break any plaquette, and it can only be detected in the lines.

the machine to really distinguish between orbits. In order to avoid these effects, the dataset is built such that it is not enough to look at one plaquette in particular, or, one (or few) plaquette(s) randomly. In order to do that, we systematically generate pairs of samples constituted by a random sample  $\mathbf{J}$  and the identical sample where we have flipped a random proportion  $q$  of the  $J_{xy}$ . As we will see later, it will be particularly difficult for the DNN to classify correctly cases where only a very small number of links were flipped. For this reason, we create two different sets of data with randomly modified couplings  $R_q(\mathbf{J})$ , using either a variable degree of changes  $q \in [1/4L^2, 0.25]$  or very similar samples, that is, changing only from 1 to 5 links. Finally, we also need to give examples of couples that do not belong to the same orbit, but where all the plaquettes are conserved, but instead large loops are not. This is the case, in particular, whenever a non connected line of couplings in the system is flipped (see  $L(\mathbf{J})$  in Fig. 2). These kinds of transformations, missed in previous works [5], play an important role when assessing the computational hardness[23]. In general, our data-set is composed of  $N_s$  couples of samples being half in the same orbit and half of different orbits. The non-gauge dataset is built using all the three transformations discussed above with equal weight.

**Construction of the DNN**— Our first goal is to understand if it possible to construct a DNN that is able to distinguish between two samples that are from the same gauge orbit or not. First, we discuss the settings. The machine we want to build should take as input a couple of samples  $\mathbf{J}$ s, and as output the probability that

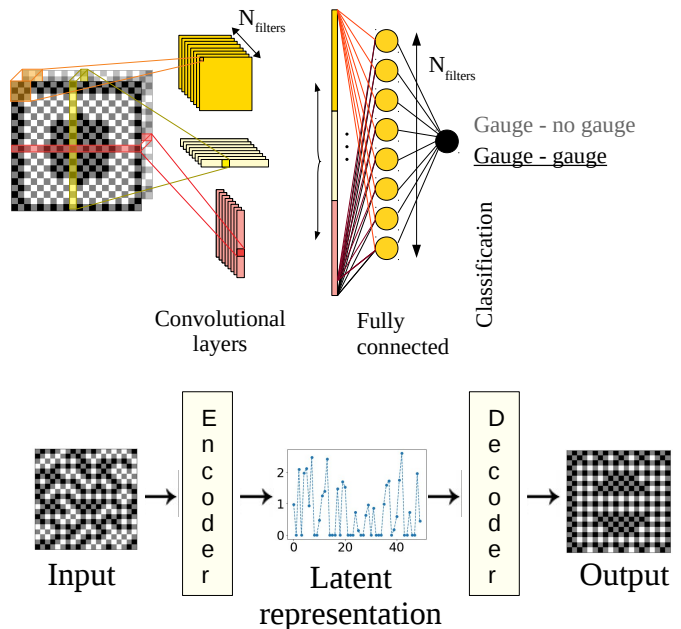


FIG. 3. (top) The typical architecture used for detecting the gauge symmetry between pairs of system. It is important to scan both square-like kernel for the plaquette and full-line kernel for the Polyakov loops. (bottom) Schematic representation of the autoencoder. The encoder is very similar to the architecture above, the decoder is typically made of upsampling layers (increasing the size of the input) and of convolutional layers.

the two samples are on the same gauge orbit or not. The geometry of the euclidean lattice of our model let us naturally make use of the convolutional neural networks (CNN) [32–34] that allows to deal with the translational symmetry. Then, we can use combinations of CNNs to catch the gauge symmetry. In particular, we should combine CNNs that scans both the plaquettes, see orange square in Fig. 3–top, and the Polyakov loops, that will be scanned by means of horizontal and vertical  $1 \times L$  slabs, see yellow and red rectangles in Fig. 3–top. The first CNN will allow us to find quickly small defects in the gauge symmetry (which are the most common), while the second would detect non local ones. In particular, we will put in parallel the three CNNs. These CNN serve as feature detectors before a fully-connected layer that performs the classification. We illustrate on Fig. 3–top how the architecture is designed in general (the number of layers and the size of the dense layer can vary depending of the considered system size), additional details and programs can be found in the SM.

**Results**— For this system, we manage to obtain almost 100% of accuracy on linear sizes of  $L = 5, 10$ . The first interesting conclusion is that it is effectively possible to learn to distinguish between pairs of samples coming from the same gauge orbit or not. We can see on Fig. 4 that the training samples on which the DNN is

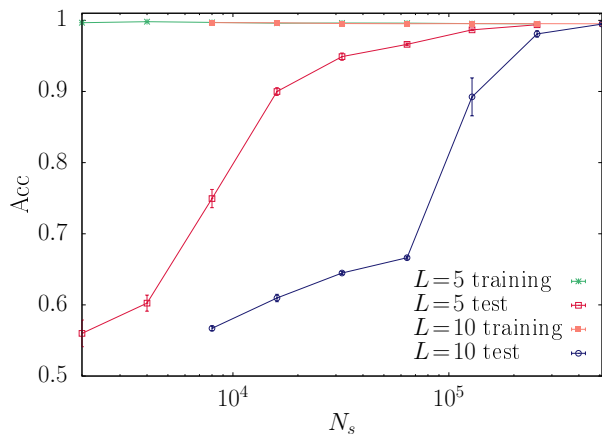


FIG. 4. General accuracy performance for the classification task of the samples in our dataset (both for the training set and for the test set). The data were averaged over 5 independent learning runs and datasets. An interesting property of the task here is that we do need a very large amount of samples in order to be able to generalize properly. In particular, it needed 10 times more samples to be able to classify the samples coming from the system of size  $L = 10$ , compared to the  $L = 5$ .

trained, rapidly converges toward 100% of correct classification, whereas on test samples (which are not seen during the training), it is necessary to use a very high amount of samples in the training in order to be able to reach such a performance. We looked at the behavior of the network specifically on samples with a given fraction of flipped couplings and on the accuracy obtained only on the samples where a whole line has been broken in order to understand how the total accuracy depends on the structure of the dataset, see Fig. 5. On the first case, we observe that in order to classify correctly the couple  $(\mathbf{J}, \mathbf{J}')$  where only  $n_l$  links have been flipped, the number of observed samples increases dramatically as  $n_l$  becomes smaller. On the second case, we see that it is clearly much harder for the network to handle the lines and therefore, the accuracy starts increasing only when taking a very high number of samples, which effectively dominates the overall accuracy shown in Fig. 4.

**Learning to fix the gauge**— We now wish to understand if a DNN can “discover” the gauge symmetry, that is, to learn to fix the gauge. For this purpose, we will make use of an auto-encoder (AE)[35, 36]. AE are a type of neural network (NN) where, an input  $x$  is encoded by a function  $f_{\mathcal{E}}$  into a latent representation, which is generally smaller than the input size. After that, a decoder maps the latent representation into a reconstructed vector  $x' = f_{\mathcal{D}}(f_{\mathcal{E}}(x))$ . One then trains the weights of the encoder and the decoder to minimize a loss function (for instance the  $L_2$  norm between  $x$  and  $x'$ ). At variance with the traditional approach, we will not ask our AE to reconstruct the input but to fix the gauge, that is to reconstruct a unique  $\hat{\mathbf{J}}$  for all the samples in the same

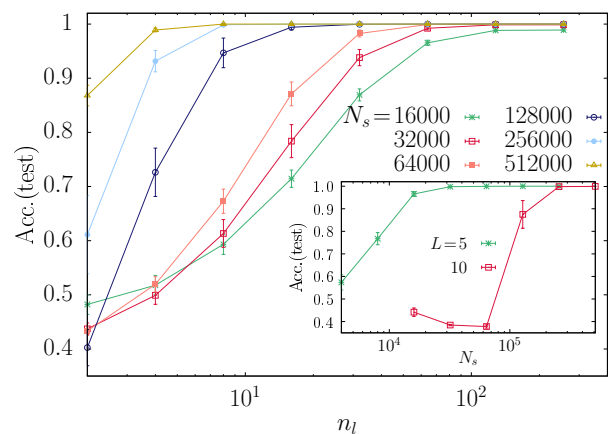


FIG. 5. Accuracy performance for the classification of non-gauge pairs coming from the two different generation procedures. **(Main panel)** Accuracy of the classification of  $L = 10$  couples formed by a sample and the same sample where  $n_l$  couplings were inverted randomly, for different number of samples used in during the training. While sample-random couples are well correctly classified even with so-few samples, one needs an exponentially larger number of samples  $N_s$  to reach a good accuracy for small number of changed links. **(Inset)** Accuracy as function of  $N_s$  for couples generated with the  $L(\mathbf{J})$  procedure for two system sizes. Clearly, learning the lines is the hardest task and dominates the performance of our machine. Curves are an average over 5 independent trainings on 5 independent datasets.

gauge orbit. One could either use a random representative of each orbit or to use our gauge fixing procedure (the comb gauge) described above. The main advantage of the latter, is that the number of variables that change over the dataset is reduced and therefore it is easier for the NN. We will use essentially the same architecture of our previous task (that is the three CNNs of Fig. 3 without the classification layer) for the encoder. The decoder takes the output of the encoder, and pipes it to an upsampling layer, followed by our three feature detector CNNs and by a last CNN from which we take the output (more details can be found in the SM). Our dataset is composed by  $N_s$  samples, each one belonging to  $N_{\mathcal{O}} \ll N_s$  different orbits. The output of each  $\mathbf{J}$  is the comb gauge of the orbit (like in Fig. 1–right).

We present results for this task on  $L = 5, 6$  and  $8$  systems averaged over 1000 test samples (that are not in the training set) in Table I. We check the accuracy of the method by comparing how different the approximate gauge-fixed output is in terms of the portion of changed links with respect to the total one,  $p$ , (i) between two samples of the same gauge orbit, (ii) two systems at random, (iii) between two samples where the second has a portion  $q$  of links flipped and (iv) between two samples where the second has a broken line. As shown in the Table I, samples from the same orbit are the only with extremely similar outputs. We can also

$L$	$N_s$	$N_{\mathcal{O}}$	$p^{J_1, O(J_1)}$	$p^{J_1, J_2}$	$p^{J_1, R_q(J_1)}, q = 0.1$	$p^{J_1, L(J_1)}$
5	100k	1k	$\sim 3\%$	$\sim 52\%$	$\sim 30\%$	$\sim 21\%$
6	400k	1k	$\sim 3.5\%$	$\sim 54\%$	$\sim 27\%$	$\sim 17.5\%$
8	800k	4k	$\sim 3.1\%$	$\sim 52\%$	$\sim 30$	$\sim 10.5\%$

TABLE I. Comparison of percentage of different couplings in the “gauge-fixed” output of the AE between two different samples of the same orbit  $[p^{J_1, O(J_1)}]$ , at random  $[p^{J_1, J_2}]$ , with  $q = 0.1$  flipped links  $[p^{J_1, R_q(J_1)}]$ , or with a broken line  $[p^{J_1, L(J_1)}]$ . All numbers are normalized by the total number of couplings.

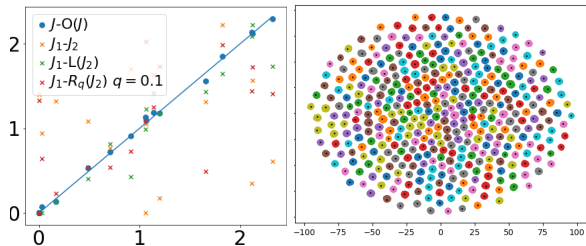


FIG. 6. On the left, a scatter plot of the latent representations of two samples from the same orbit (in blue) and two samples from different orbits (in orange, green and red). The green dots correspond to a sample differing by a whole line, and the red ones by  $q = 0.1$  couplings changed. On the right (in arbitrary units), illustration of the latent encoding for many orbit gauges for the  $L = 5$  system. Each color/blob corresponds to samples coming from the same gauge orbit. The black dot is the latent representation of the comp gauge of the orbit. We clearly see that each orbit form a cluster that is well separated from the rest.

check whether the latent representation (of test samples and orbits) can cluster together samples from orbits together in the same orbit. On Fig. 6-left, we compare the latent representation of samples from the same gauge orbit or not and, on the right side, we use the t-sne tool[37] to visualize in two-dimension the latent representation. Our machine clearly succeeds in finding a good latent representation for the orbit: we see that the latent representation is very close for two samples from the same orbit, whereas even a slight change of a few plaquettes, or of one line makes a noticeable difference.

We have shown a successful machine learning approach to detect gauge symmetries. This problems is a particular challenge for neural networks because no single local or global order parameter is available. In fact, we see that naive standard approaches using pre-trained deep neural networks fail to tell us if two samples are or not a gauge transformation one from the other, even if we can generate arbitrary large training sets. Our results underline the necessity of being very careful with the dataset used for the learning phase if we want the NN to learn the full symmetry and that one needs to force the machine to look on the same footing local and global loops. We

show that our NN are able to learn the gauge symmetry and even to fix the gauge and cluster samples in orbits, however at the cost of very large training datasets as compared to the system sizes. Now that we have NNs able to see gauge symmetries and find a latent representation for the orbits, we will approach our original motivation, using these machines to understand what makes certain samples computationally far more costly than others.

We thank L. A. Fernández for encouraging discussions and Marco Baity-Jesi for his careful reading of the manuscript. This work was partially supported by Ministerio de Economía, Industria y Competitividad (MINECO) (Spain) through Grant No. FIS2015-65078-C2 (also partly funded by the EU through the FEDER program) and by the LabEx CALSIMLAB (public grant ANR-11-LABX-0037-01 constituting a part of the “Investissements d’Avenir” program - reference : ANR-11-IDEX-0004-02).

- [1] D. Silver, A. Huang, C. J. Maddison, A. Guez, L. Sifre, G. van den Driessche, J. Schrittwieser, I. Antonoglou, V. Panneershelvam, M. Lanctot, S. Dieleman, D. Grewe, J. Nham, N. Kalchbrenner, I. Sutskever, T. Lillicrap, M. Leach, K. Kavukcuoglu, T. Graepel, and D. Hassabis, *Nature* **524**, 484 (2016).
- [2] Y. LeCun, Y. Bengio, and G. Hinton, *Nature* **521**, 436 (2015).
- [3] J. Schmidhuber, *Neural Networks* **61**, 85 (2015).
- [4] G. Torlai and R. G. Melko, *Phys. Rev. B* **94**, 165134 (2016).
- [5] J. Carrasquilla and R. G. Melko, *Nature Physics* **13**, 431 (2017).
- [6] S. J. Wetzel and M. Scherzer, *Physical Review B* **96**, 184410 (2017).
- [7] E. van Nieuwenburg, Y.-H. Liu, and S. Huber, *Nature Physics* **13**, 435 (2017).
- [8] L. Wang, *Phys. Rev. B* **94**, 195105 (2016).
- [9] T. Ohtsuki and T. Ohtsuki, *Journal of the Physical Society of Japan* **86**, 044708 (2017), <https://doi.org/10.7566/JPSJ.86.044708>.
- [10] M. J. S. Beach, A. Golubeva, and R. G. Melko, *Phys. Rev. B* **97**, 045207 (2018).
- [11] S. S. Schoenholz, E. D. Cubuk, D. M. Sussman, and E. Kaxiras, *Nature Physics* **12**, 469 (2016).
- [12] S. S. Schoenholz, E. D. Cubuk, E. Kaxiras, and A. J. Liu, *Proceedings of the National Academy of Sciences* **114**, 263 (2017), <https://www.pnas.org/content/114/2/263.full.pdf>.
- [13] E. D. Cubuk, S. S. Schoenholz, J. M. Rieser, B. D. Malone, J. Rottler, D. J. Durian, E. Kaxiras, and A. J. Liu, *Phys. Rev. Lett.* **114**, 108001 (2015).
- [14] D.-L. Deng, X. Li, and S. Das Sarma, *Phys. Rev. B* **96**, 195145 (2017).
- [15] M. Koch-Janusz and Z. Ringel, *Nature Physics* **14**, 578 (2018).
- [16] S. Elitzur, *Phys. Rev. D* **12**, 3978 (1975).
- [17] F. Barahona, *Journal of Physics A: Mathematical and General* **15**, 3241 (1982).

- [18] S. Istrail, in *Proceedings of the thirty-second annual ACM symposium on Theory of computing - STOC '00* (ACM Press, New York, New York, USA, 2003) pp. 87–96.
- [19] R. Alvarez Baños, A. Cruz, L. A. Fernandez, J. M. Gil-Narvion, A. Gordillo-Guerrero, M. Guidetti, A. Maiorano, F. Mantovani, E. Marinari, V. Martín-Mayor, J. Monforte-Garcia, A. Muñoz Sudupe, D. Navarro, G. Parisi, S. Perez-Gavero, J. J. Ruiz-Lorenzo, S. F. Schifano, B. Seoane, A. Tarancon, R. Tripiccion, and D. Yllanes (Janus Collaboration), *J. Stat. Mech.* **2010**, P06026 (2010), arXiv:1003.2569.
- [20] L. A. Fernández, V. Martín-Mayor, G. Parisi, and B. Seoane, *EPL (Europhysics Letters)* **103**, 67003 (2013).
- [21] A. Billoire, *J. Stat. Mech.* **2014**, P04016 (2014), arXiv:1401.4341.
- [22] V. Martín-Mayor and I. Hen, *Scientific Reports* **5**, 15324 (2015), arXiv:1502.02494.
- [23] L. Fernandez, E. Marinari, V. Martin-Mayor, G. Parisi, and D. Yllanes, *Journal of Statistical Mechanics: Theory and Experiment* **2016**, 123301 (2016).
- [24] A. Billoire, L. A. Fernandez, A. Maiorano, E. Marinari, V. Martin-Mayor, J. Moreno-Gordo, G. Parisi, F. Ricci-Tersenghi, and J. J. Ruiz-Lorenzo, *Journal of Statistical Mechanics: Theory and Experiment* **2018**, 033302 (2018).
- [25] Actually, Refs. [19–21, 23, 24] attempted to find equilibrium configurations using a Parallel Tempering algorithm down to some minimal temperature  $T_{\min}$ . In order to compute the Ground State, one needs to push  $T_{\min}$  to zero, as done for instance in Ref. [22]. Unfortunately, the lower  $T_{\min}$  the larger the spread over the samples of the computational hardness, see e.g. Refs. [19, 23, 24].
- [26] G. Toulouse, *Communications on Physics* **2**, 115 (1977).
- [27] K. He, X. Zhang, S. Ren, and J. Sun, in *Proceedings of the IEEE conference on computer vision and pattern recognition* (2016) pp. 770–778.
- [28] I. Montvay and G. Münster, *Quantum Fields on a Lattice* (Cambridge University Press, Cambridge, 1997).
- [29] F. Chollet *et al.*, “Keras,” <https://keras.io> (2015).
- [30] F. Pedregosa, G. Varoquaux, A. Gramfort, V. Michel, B. Thirion, O. Grisel, M. Blondel, P. Prettenhofer, R. Weiss, V. Dubourg, J. Vanderplas, A. Passos, D. Cournapeau, M. Brucher, M. Perrot, and E. Duchesnay, *Journal of Machine Learning Research* **12**, 2825 (2011).
- [31] In this work we deal with an abelian gauge group which makes it possible, fixing the Gauge for non-abelian gauge group is a non-trivial problem, see Ref. [38].
- [32] K. Fukushima, *Biological cybernetics* **36**, 193 (1980).
- [33] Y. LeCun, B. Boser, J. S. Denker, D. Henderson, R. E. Howard, W. Hubbard, and L. D. Jackel, *Neural computation* **1**, 541 (1989).
- [34] A. Krizhevsky, I. Sutskever, and G. E. Hinton, in *Advances in neural information processing systems* (2012) pp. 1097–1105.
- [35] D. E. Rumelhart, G. E. Hinton, and R. J. Williams, *Learning internal representations by error propagation*, Tech. Rep. (California Univ San Diego La Jolla Inst for Cognitive Science, 1985).
- [36] D. H. Ballard, in *AAAI* (1987) pp. 279–284.
- [37] L. v. d. Maaten and G. Hinton, *Journal of machine learning research* **9**, 2579 (2008).
- [38] E. Marinari, C. Parrinello, and R. Ricci, *Nuclear Physics B* **362**, 487 (1991).